ADVANCED MATERIALS
www.advmat.de

Fluorinated Graphene for Promoting Neuro-Induction of Stem Cells

Yu Wang, Wong Cheng Lee, Kiran Kumar Manga, Priscilla Kailian Ang, Jiong Lu, Yan Peng Liu, Chwee Teck Lim, and Kian Ping Loh**

Stem cells play a pivotal role in the human body by providing a repair system for organs and tissues needed for their continual growth and renewal throughout ontogeny. Stem cells are now used as an integral part of modern clinical treatment.[1] Intensive research has been carried out on stem cells to understand the complex molecular and cellular events occurring during early development, disease progression, epigenetics, and pathophysiology.[2] Bone marrow derived mesenchymal stem cells (MSCs) have the potential to differentiate into tissues of mesenchymal origin including adipocytes, osteoblasts and chondrocytes.[3] Whilst MSCs were initially believed to be restricted to the mesenchymal lineages, recent evidence suggests that MSCs can trans-differentiate into tissues of non-mesenchymal origin such as the neurons. This has generated great interests about the potential use of MSCs for the treatment of degenerative and autoimmune diseases of the nervous system.[4,5] However, the mechanisms and the process of trans-differentiation of MSCs to neurons are still not well understood and the occurrence of full functional neural differentiation is still debatable.[6]

Surface chemistry plays an important role in terms of the adhesion properties of proteins and cells. These are mediated at the molecular level by specific functional groups like amine, carboxylic acid and hydroxyl groups. Surfaces with good biocompatibility and tissue-specific inductive capabilities are highly desirable in various tissue engineering and cell therapeutic applications. Previous work has shown that graphene and graphene oxide (GO)[7] can influence cell behaviour, including attachment, growth, proliferation and differentiation, due in part to its aromatic scaffold which can increase the local concentration of extracellular matrix (ECM) such as collagen, laminin and fibronectin by non-covalent binding. It is interesting to consider fucntionalized graphene such as fluorinated graphene,[8] which is distinct from its polymeric analog such as PTFE due to its highly directional and polar bonding on the surface. The strong polarity of the carbon-fluorine bond is expected to induce biological responses.[9] For example, the introduction of fluorine into pharmaceutical drugs improves metabolic stability and increase the strength of interaction with targeted proteins.[10] The presence of fluorine affects the properties of molecules due to its high electronegativity and small size. Thus, approximately 30% of all agrochemicals and 20% of all pharmaceuticals drugs contain fluorine,[10] including drugs such as Lipitor, Lexapro and Prozac.

In this work, we used fluorinated graphene sheets as the scaffold for stem cell growth. Changes in cellular adhesion, morphology, gene expression and differentiation have been rationalised in terms of the surface chemistry, topography and mechanical properties of the substrate on which the cells have been cultured. Our results showed that fluorinated graphene (FG) induced higher proliferation and stronger polarization of MSCs. Morphological changes in terms of cytoskeletal and nuclear alignment promote the differentiation of MSCs towards the neuronal lineage and the effect can be further enhanced with the addition of neuron-inductive agent, retinoic acid. More importantly, by leveraging on alignment induced neuronal differentiation, the stem cells can be controllably patterned on fluorinated graphene, pointing to a large-scale and rapid strategy to align MSCs and the ability to induce neuronal lineage in the absence of chemical inducer.

The fluorination of graphene was performed by exposing the samples to a fluorinating agent, Xenon difluoride (XeF_2, from Alfa Aesar). The coverage of fluorine on the graphene sample can be controlled by the exposure time in XeF_2 atmosphere. Raman spectroscopy, X-ray Photoelectron Spectroscopy (XPS) and High Resolution Electron Energy Loss Spectroscopy (HREELS) were carried out to evaluate the bonding states of carbon atoms in graphene following the fluorination. The Raman spectra (514 nm) collected for pristine and fluorinated graphene on SiO_2/Si substrates for different length of fluorination times are shown in **Figure 1**a. The pristine graphene shows the characteristic G (~1587 cm^{-1}) and 2D (~2688 cm^{-1}) band. With increasing fluorination time, a D-band induced by defects or sp^3 bonding emerges at 1350 cm^{-1}, while a new peak (~1618 cm^{-1}) splits off from the G band (called D' peak) and the intensity of the 2D band decreases. These new features are analogous to the formation of sp^3 graphane phases and are well documented.[11] When the exposure time is extended to 3600s, the characteristic Raman peaks of pristine graphene completely disappears. This indicates that the aromatic π-electron conjugation

Dr. Y. Wang,[†] K. K. Manga, P. K. Ang, J. Lu, Y. P. Liu, Prof. K. P. Loh
Graphene Research Centre and Department of Chemistry
National University of Singapore
3 Science Drive 3, 117543, Singapore
E-mail: chmlohkp@nus.edu.sg
W. C. Lee,[†] Prof. C. T. Lim
Department of Bioengineering and Department of Mechanical Engineering
Mechanobiology Institute
National University of Singapore
7 Engineering Drive 1, 117574, Singapore
E-mail: ctlim@nus.edu.sg
[†] These authors contributed equally to this work.

DOI: 10.1002/adma.201200846

ADVANCED MATERIALS
www.advmat.de

www.MaterialsViews.com

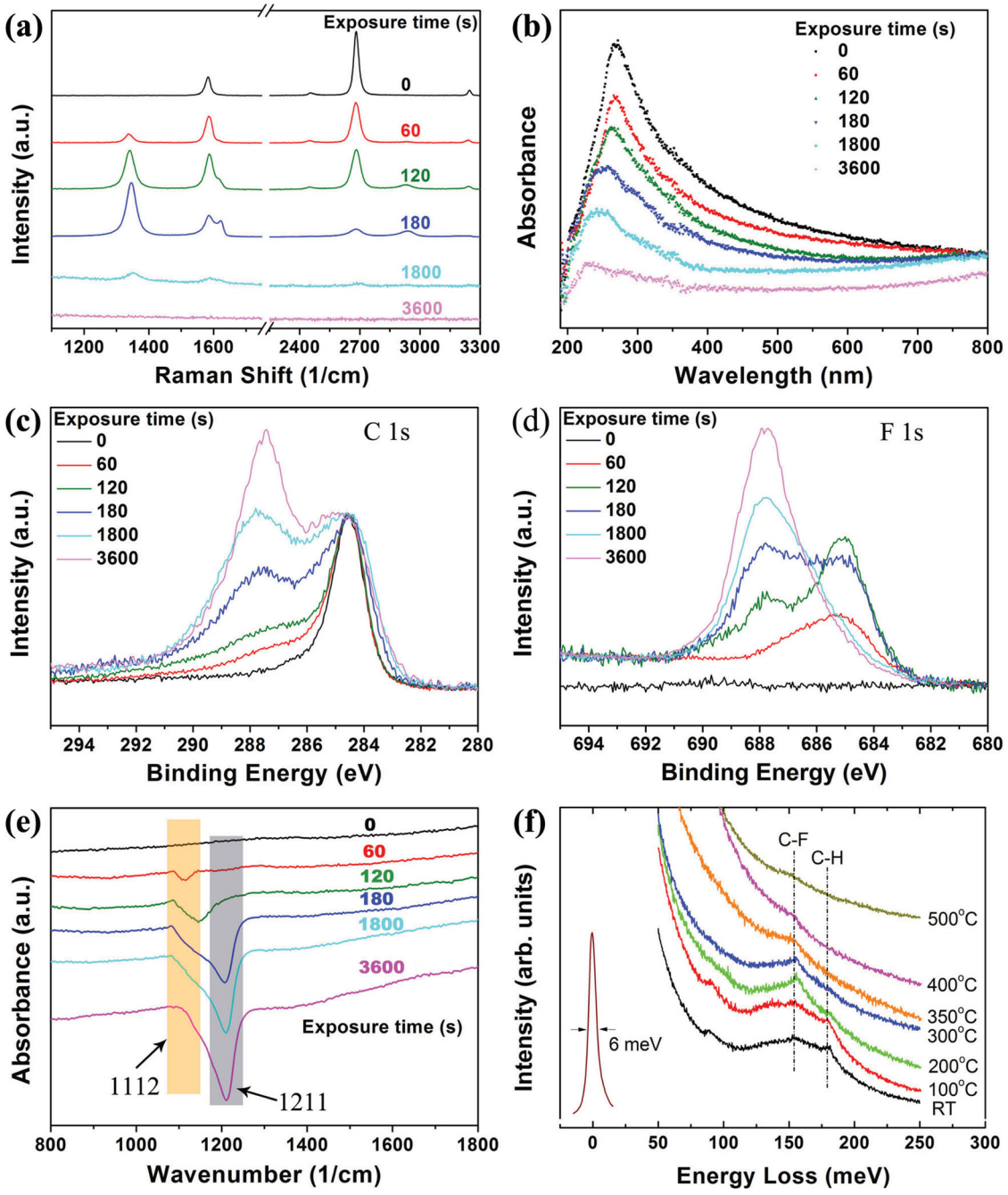

Figure 1. Evolution of C-F phases on graphene with increasing exposure time to XeF_2 characterized by (a) Raman spectra (514 nm), (b) UV-Visible spectra, (c, d) XPS C1s and F 1s core-level spectra, and (e) FT-IR spectra. (f) HREELS showing defluorinaion of fluorographene by thermal annealing.

is totally destroyed, due to the double-sided functionalization of the graphene sheet.[8] At this point, a characteristic ratio of 50% F/C peak intensity in the XPS spectra is designated as double-side fluorinated graphene.[12] UV-vis spectroscopy was used also to probe for the effect of fluorination on π-bonded electronic configuration of graphene. The spectrum of pristine graphene shows a single broad absorption peak at 270 nm which is characteristic of π–π^* electron transition in the aromatic system of graphene film. After fluorination, a blue shift (~43 nm) is found because of the polarization-induced charge effect.[13] The XPS C1s and F1s spectra of the fluorinated graphene are shown in Figure 1c and 1d, respectively. The carbon peak is observed at 284.6 eV for the pristine graphene sample, while a chemically shifted component at ~287.5 eV can be assigned to the C-F binding state by comparison with literature data on fluorinated graphite.[14] From the F 1s spectra, we find the C-F bond type changes from 'semi-ionic' (685.5 eV binding energy) to covalent (687.5 eV binding energy) with increasing fluorination

DOI: 10.1002/adma.201200846

degree.[15] As shown also in the FTIR spectra in Figure 1e, with increasing fluorination time, an absorption band at 1112 cm^{-1} related to the 'semi-ionic' C-F bonds gradually changes into a strong band at 1211 cm^{-1} attributable to covalent C-F bonding.

The stability of fluorinated graphene was monitored by annealing the substrate in vacuum and observing how the C-F changes using high-resolution electron energy loss spectroscopy (HR-EELS). In Figure 1f, the loss peak at around 154 meV, which is attributed to the C-F bond, can be clearly observed after annealing the surface at 300 °C for 1 h (1.0×10^{-10} Torr). This suggests the fluorinated graphene has good thermal stability. The fluorographene can be completely de-fluorinated after heating above 500 °C.

Human bone marrow derived MSCs were cultured on fluorinated graphene (quartz as substrate) and as-grown graphene was used as control. We first compare the morphology and proliferation of MSCs plated on the substrates in basal growth medium and monitored their cell density over a period of 7 days. Fluorescent images of MSCs on graphene (**Figure 2**a), partially fluorinated graphene (PFG) (Figure 2b) and fully fluorinated graphene (FG) substrates (Figure 2c) display distinctive differences in cell morphology and density. The actin cytoskeletal filaments were stained with phalloidin and observed under an epi-fluorescence microscope. As shown in Figure 2c, MSCs cultured on FG proliferate faster and reach high confluence on day 7 as compared to those cultured on PFG and G. The full fluorination of graphene achieves a nearly three-fold increase in cell density, showing that the introduction of C-F bonding on the surface of graphene facilitates better cell adhesion and proliferation (Figure 2d). MSCs on FG are more spindly and elongated which can be attributed to the high density and close packing of the cells. The F-actin fibers are mostly stretched along the long axis of the cells. In contrast, MSCs cultured on PFG and G are less elongated and more widespread.

Previous studies have shown that hydrophilic graphene oxide (GO) can bind to serum proteins *via* electrostatic interactions, which contributes to a higher density of adhesion molecules available for cell attachment and growth.[16] In the case of C-F bonds, it is expected that electrostatic interactions play an important role in determining the biological response to surfaces.[17] To investigate the relationship between the surface of fluorinated graphene and the controlled growth of MSCs on

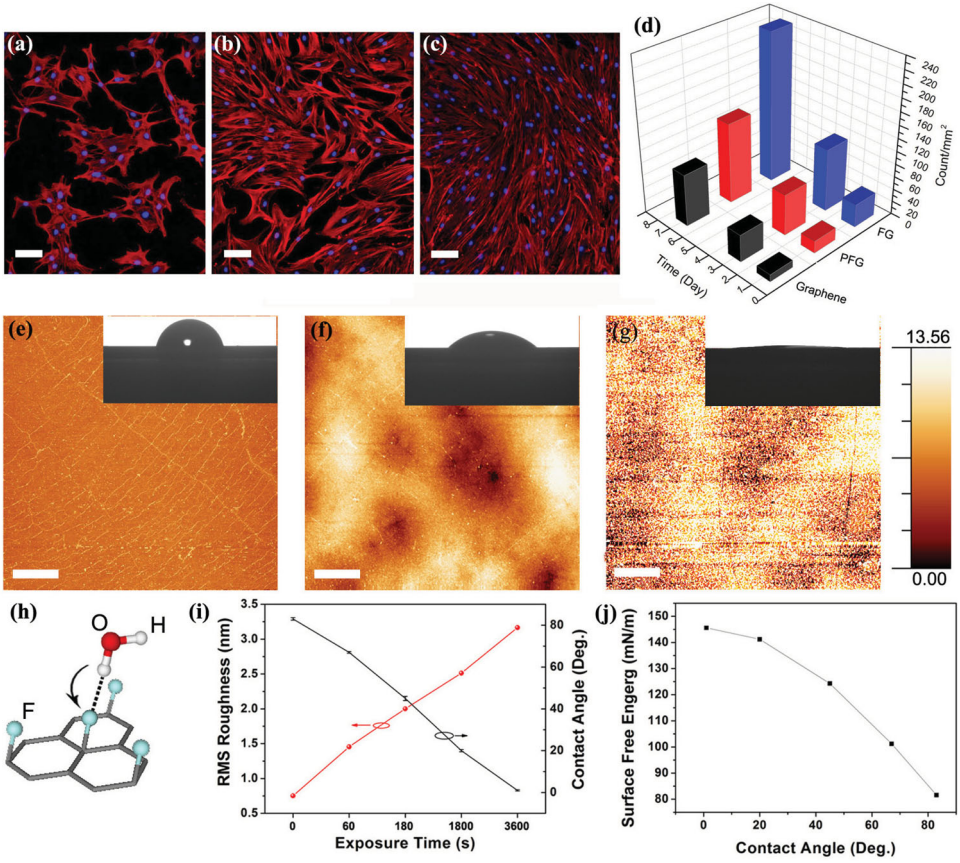

Figure 2. (a–c) Fluorescent images of actin cytoskeleton of MSCs cultured on graphene, PFG and FG stained with rhodamine-phalloidin at day 7 (scale bar = 100 μm). (d) Proliferation of MSCs cultured on the graphene films, showing the controlled growth of MSCs on fluorinated graphene with different coverage of fluorine. (e–g) AFM images of graphene, PFG and FG, respectively, show the surface of fluorinated graphene (scale bar = 5 μm). The insets correspond to the measurement of water contact angle. (h) Description of the hyperconjugative interaction in this complex in terms of resonance theory illustrating effective charge transfer from H-bond acceptor (water) to H–bond donor (F–graphene). (i) Roughness and water contact angle as a function of exposure time for graphene fluorination. (j) Surface free energy (γ_{SL}) of fluorinated graphene films.

it, the morphology and wettability of surfaces were measured by atomic force microscopy (AFM) and water contact angle (WCA), respectively. With increasing surface coverage of fluorine, the root mean square (RMS) roughness increases from 0.75 nm (graphene) to 3.16 nm (fully fluorinated graphene). After full fluorination, the water contact angle of graphene surface reduces from 83° to ~1° (The insets in Figure 2e–g). The lower contact angle of water is caused by a decrease in the free surface energy of the solid/liquid interface (γ_{SL}) resulting from hydrogen bonding.[18] In Figure 2j, the surface free energy of samples is calculated by the Owens-Wendt model: $\gamma_{SL} = (1+\cos\theta)\gamma_L$, where γ_{SL} is the solid-liquid interfacial energy; θ is the contact angle; the surface tension of deionized water (γ_L, mN m^{-1}) at 20 °C is 72.8 from Lamour *et al.*[19] The conventional hydrophobicity of fluorinated surfaces is due to the inefficient packing of fluorocarbons on surfaces, leading to poor hydrogen bonding or long range dipole-dipole interactions with water molecules.[20] Theoretical calculation and experiments demonstrated that fluorine coverage saturates at C_4F for one-sided full fluorination, which corresponds to one fluorine atom every two primitive graphene unit cells.[8] Such high coverage of fluorine atoms on a single sheet of carbon present an ordered array of oriented dipoles that can interact with the molecular dipoles of water. Meanwhile, H-bonding interactions also contribute to the decrease of the measured water contact angle. Although the fluorine lone pairs are in conjugation with the local π–orbital system of graphene, C-F···H-O interaction may result from a balance of hyperconjugative bond weakening and rehybridization promoted bond strengthening (Figure 2h).[21] This is in good agreement with the increased wetting properties of fluorinated PDMS surface treated by low pressure CF_4 plasma.[22]

Recent works have demonstrated that MSC lineage specification and cell maturation can be directed by various physical stimuli such as substrate stiffness and cell shape.[23,24] The mechanical tension induces changes in the dynamic and organization of many intra-cellular structures, thereby resulting in changes in gene and protein expression and the phenotype of MSCs. Since cytoskeleton and nucleus elongation is known to induce neuronal differentiation,[25] the elongation index (E) of the nucleus of the cells plated on FG and G is measured using tissue culture polystyrene (PS) as control (Seeing Supporting Information). Based on the statistical results, the nulceus elongation of MSCs cultured on FG is signifcantly higher than those cultured on G and PS (*$p < 0.05$).

The observed differences could be attributed to the polarization effect of the carbon-fluorine bond which may facilitate cell alignment and nucleus elongation through electrostatic induction at the interface of cell-FG. In addition to morphological changes, neuronal markers- Tuj1 and MAP2, are highly expressed in MSCs cultured on FG as shown by the immunofluorescence staining (**Figure 3**a). However, co-expression of Nestin is weak in all samples (Figure 3b). The glial specific marker-Glial-fibrillary acidic protein (GFAP) is weakly detected, suggesting a preference of morphological induced differentiation towards the neuronal lineage over the glial lineage. We note that at day 21, compared with the MSCs cultured on G and PS, MSCs cultured on FG demonstrated neuron-like morphologies with visible neurite protrusions indicating further neuronal maturation (see Supporting Information).

Neuronal differentiation of MSCs has been extensively studied and garnered wide interest in the fields of tissue engineering and cell therapy due to their ready availability from the donor bone marrow.[26] To further enhance neuronal differentiation of MSCs, we examined the expression of neuronal gene markers in the neuronal induction culture with retinoic acid. The expression of neuronal markers- Tuj1 and MAP2 was further enhanced when the MSCs were cultured in the presence of 30 µM of retinoic acid (Figure 3b and 3e). The expression of GFAP was slightly enhanced for the MSCs cultured on FG (Figure 3c). Our results show that FG promotes the

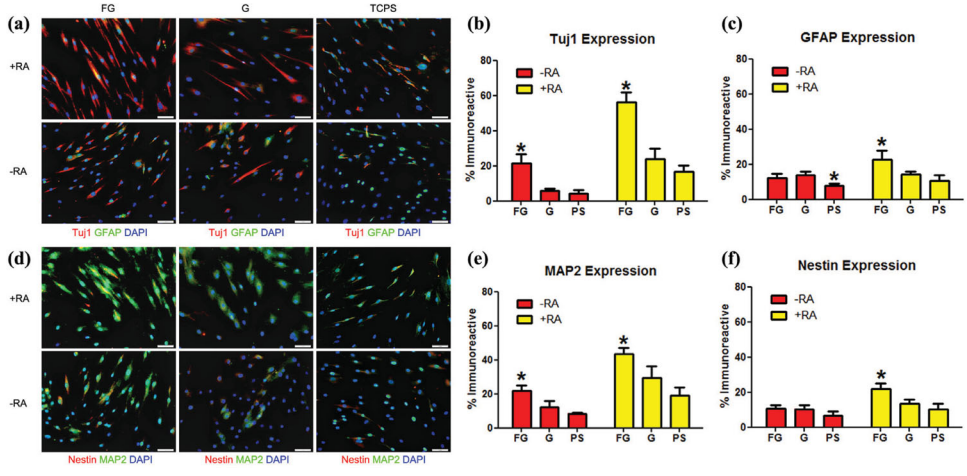

Figure 3. Fluorescent images of immunostained MSCs for (a) Tuj1 and GFAP and (d) Nestin and MAP2cultured on FG, G and PS in the presence of retinoic acid (+RA) and in the absence of retinoic acid (-RA). (a) Tuj1 is shown in red, GFAP in green and (d) Nestin is shown in red, MAP2 is shown in green. Cell nucleus is counter-stained with DAPI in blue (scale bar = 100 µm). Representative areas of the samples were taken. Percentage of immunoreactive MSCs for (b) Tuj1 (c) GFAP, (e) MAP2 and (f) Nestin on FG, G and PS. Note that more MSCs expressed Tuj1 and MAP2 when cultured on FG and the expression level is further enhanced with the addition of retinoic acid. ($n = 6$, *$p < 0.05$).

Adv. Mater. **2012**,
DOI: 10.1002/adma.201200846

neuronal differentiation of MSCs and the effect could be further enhanced with the addition of neuron-inductive agent.

In addition to chemical effect, biomechanical signals can also be transmitted to cells *via* various substrate topographical features such as pillars, grooves or pits.[27] The physical or mechanical stimuli alone is increasingly considered to be sufficient in specifying stem cell lineages which might alleviate the need for chemical factor stimulation. Since distinct morphological characteristics often accompany stem cell differentiation, we investigated whether enhanced neural differentiation can be induced by confining the MSCs into microchannels of FG in the absence of chemical inducers. In **Figure 4**a, polydimethylsiloxane (PDMS diluted in hexane was utilized as ink) lines were ink-jet printed onto the fluorinated graphene substrates, using a GIX Microplotter II inkjet printer. A typical optical microscopic image of the printed PDMS lines is shown in Figure 4b. The printed PDMS lines have lengths of 3 mm and widths of 150 µm with a line spacing of ~50 µm resulting in a 30 µm wide FG microchannel in between the PDMS lines. It can be seen in Figure 4c to 4e that the density of aligned MSCs correlates with the coverage of fluorine on the graphene film. Interestingly, randomly seeded MSCs preferentially attach onto the FG microchannels and assume a more elongated morphology. MSCs were cultured on the micro-patterns for 14 days and the expression of neuronal markers analyzed. The morphology of MSCs was examined by F-actin staining. As shown in Figure 4f and Figure 4g, MSCs preferentially adhere onto the FG strips and their cytoskeleton aligns along the length of the pattern. Compared with the cells cultured under non-patterned FG, those cultured in 30 µm FG microchannels demonstrate enhanced expression of Tuj1 and MAP2 even in the absence of neuron-inductive agent (Figure 4h). We note that our finding is consistent with the work by Leong and co-workers demonstrating that cytoskeletal and nuclear alignment promote spontaneous neural differenatiation and that the effect could be combined with chemical cues to create a synergistic condition to further enhance the differentiation.[25]

In conclusion, engineering substrates to induce desired cell phenotype and genotype is an important strategy of scaffold design for tissue-engineering applications. In the present study, we demonstrated that fluorinated graphene can be used to enhance cell adhesion and proliferation of MSCs, and it exhibits a neuro-inductive effect *via* spontaneous cell polarization. Fluorinated graphene films are found to be highly supportive of MSCs growth and the coverage of fluorine has significant effects on cell morphology, cytoskeletal and nuclear elongation of MSCs. Through a rapid and large-area ink-jet printing method, we also demonstrated enhanced neurogenesis *via* channel confined cell elongation in the absence of chemical factor stimulation. Our work shows that fluorinated graphene

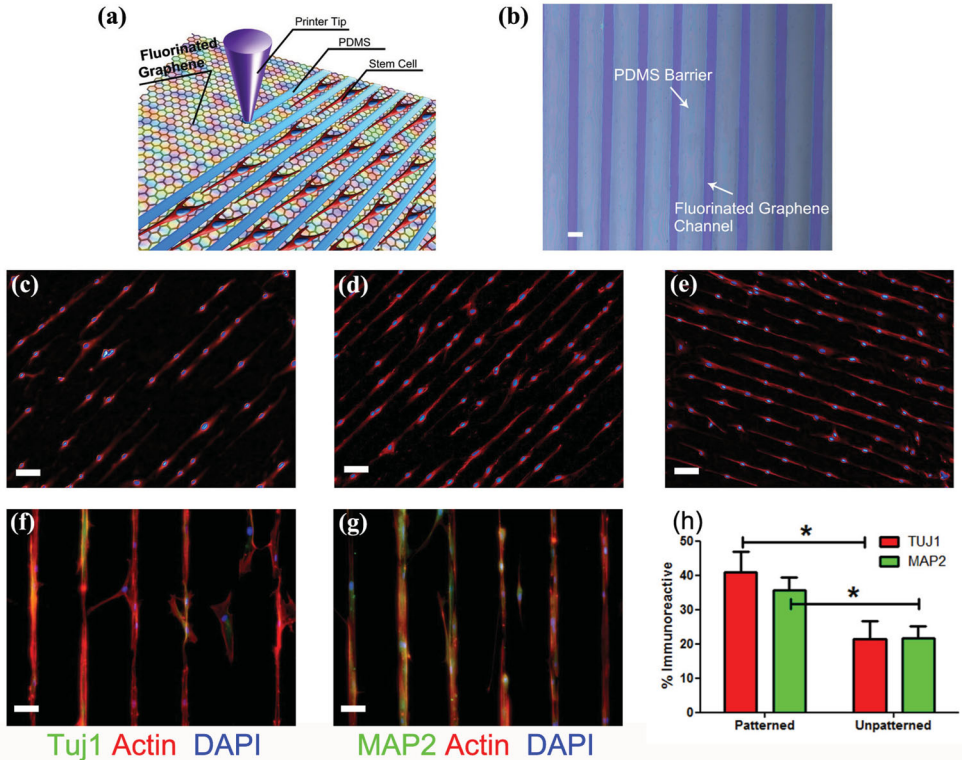

Figure 4. (a) Schematic drawing of patterning MSCs by printing PDMS barriers on graphene films directly. (b) Optical microscope image of printed PDMS on fluorinated graphene film (scale bar = 50 µm). (c–e) The aligned growth of stem cell on graphene, PFG and FG with printed PDMS pattern, respectively (scale bar = 100 µm). (f, g) MSCs preferentially attached on the FG strips and their F-actin aligned (red) and expressed neural specific markers- Tuj1 and MAP2 (green) (scale bar = 50 µm). (h) Percentage of immunoreactive cells for Tuj1 and MAP2 on unpatterned and patterned FG strips. Note that the patterned FG strips induce higher expression of Tuj1 and MAP2 in the absence of retinoic acid. ($n = 6$, $p < 0.05$).

sheets, produced in large scaled and patterned, may be a viable platform for tissue-engineering applications.

Experimental Section

Cell Culture: Human bone marrow derived MSCs were obtained from commercial sources (Lonza) and cultured accroding their to recommended standard protocol. Details are provided in the Supporting Information.

Supporting Information

Supporting Information is available from the Wiley Online Library or from the author.

Acknowledgements

We thank the financial support of NRF-CRP award "Graphene and Related Materials and Devices" R-143-000-360-281.

Received: February 29, 2012
Revised: March 17, 2012
Published online:

[1] S. I. Nishikawa, L. M. Jakt, T. Era, *Nat. Rev. Mol. Cell Biol.* **2007**, *8*, 502.
[2] L. Li, T. Xie, *Annu. Rev. Cell Dev. Biol.* **2005**, *21*, 605.
[3] M. F. Pittenger, A. M. Mackay, S. C. Beck, R. K. Jaiswal, R. Douglas, J. D. Mosca, M. A. Moorman, D. W. Simonetti, S. Craig, D. R. Marshak, *Science* **1999**, *284*, 143.
[4] Y. Jiang, D. Henderson, M. Blacksta, A. Chen, R. F. Miller, C. M. Verfaillie, *Proc. Natl. Acad. Sci. USA.* **2003**,*100*, 11854.
[5] S. Bonilla, A. Silva, L. Valdes, E. Geijo, J. M. Garcia-Verdungo, S. Martinez, *Neuroscience* **2005**, *133*, 85.
[6] M. Krampera, S. Marconi, A. Pasini, M. Galie, G. Rigotti, F. Monsa, M. Tinelli, L. Lovato, E. Anghileri, A. Andreini, G. Pizzolo, A. Sbarbati, B. Bonetti, *Bone* **2007**, *40*, 382.
[7] H. Q. Chen, M. B. Müller, K. J. Gilmore, G. G. Wallace, D. Li, *Adv. Mater.* **2008**, *20*, 3557.
[8] J. T. Robinson, J. S. Burgess, C. E. Junkermeier, S. C. Badescu, T. L. Reinecke, F. K. Perkins, M. K. Zalalutdniov, J. W. Baldwin, J. C. Culbertson, P. E. Sheehan, E. S. Snow, *Nano Lett.* **2010**, *10*, 3001.
[9] M. P. Lutolf, J. A. Hubbell, *Nat. Biotechnol.* **2005**, *23*, 47.
[10] K. Müller, C. Faeh, F. Diederich, *Science* **2007**, *317*, 1881.
[11] D. C. Elias, R. R. Nair, T. M. G. Mohiuddin, S. V. Morozov, P. Blake, M. P. Halsall, A. C. Ferrari, D. W. Boukhvalov, M. I. Katsnelson, A. K. Geim, K. S. Novoselov, *Science* **2009**, *323*, 610.
[12] Y. S. Lee, T. H. Cho, B. K. Lee, J. S. Rho, K. H. An, Y. H. Lee, *J. Fluorine Chem.* **2003**, *120*, 99.
[13] E. Burstein, *Phys. Rev.* **1954**, *93*, 632.
[14] T. Nakajima, (ed.) *Fluorine-Carbon and Fluoride-Carbon Materials,* Marcel-Dekker, New York **1995**.
[15] C. P. Ewels, G. V. Lier, J. C. Charlier, M. I. Heggie, P. R. Briddon, *Phys. Rev. Lett.* **2006**, *96*, 216103.
[16] W. C. Lee, C. H. Y. X. Lim, H. Shi, L. A. L. Tang, Y. Wang, C. T. Lim, K. P. Loh, *ACS Nano* **2011**, *5*, 7334.
[17] Y. Mei, S. Gerecht, M. Taylor, A. J. Urquhart, S. R. Bogatyrev, S. W. Cho, M. C. Davies, M. R. Alexander, R. S. Langer, D. G. Anderson, *Adv. Mater.* **2009**, *21*, 2781.
[18] J. Rafiee, X. Mi, H. Gullapalli, A. V. Thomas, F. Yavari, Y. Shi, P. M. Ajayan, N. A. Koratkar, *Nat. Mater.* **2012**, *11*, 217.
[19] G. Lamour, A. Eftekhari-Bafrooei, E. Borguet, S. Souès, A. Hamraoui, *Biomaterials* **2010**, *31*, 3762.
[20] V. H. Dalvi, P. J. Rossky, *Proc. Natl. Acad. Sci. USA* **2010**, *107*, 13603.
[21] I. V. Alabugin, M. Manoharan, S. Peabody, F. Weinhold, *J. Am. Chem. Soc.* **2003**, *125*, 5973.
[22] A. L. Cordeiro, M. Nitschke, A. Janke, R. Helbig, F. D'Souza, G. T. Donnelly, P. R. Willemsen, C. Werner, *Express Polym. Lett.* **2009**, *3*, 70.
[23] L. Gao, R. McBeath, C. S. Chen, *Stem Cells* **2010**, *28*, 564.
[24] A. J. Engler, S. Sen, H. L. Sweeney, D. E. Discher, *Cell* **2006**, *126*, 677.
[25] E. K. F. Yim, S. W. Pang, K. W. Leong, *Exp. Cell. Res.* **2007**, *313*, 1820.
[26] B. R. Snyder, A. M. Chiu, D. J. Prockop, A. W. S. Chan, *Plos One* **2010**, *5*, e9347.
[27] R. G. Flemming, C. J. Murphy, G. A. Abrams, S. L. Goodman, P. F. Nealey, *Biomaterials* **1999**, *18*, 1573.